Research Article | Vol. 30, No. 7 / 28 Mar 2022 / Optics Express 12026
Optics EXPRESS

Simultaneous modal phase and group velocity matching in microstructured optical fibers for second harmonic generation with ultrashort pulses

ARTEMII TISHCHENKO,* THOMAS GEERNAERT, NATHALIE VERMEULEN, FRANCIS BERGHMANS, AND TIGRAN BAGHDASARYAN

Vrije Universiteit Brussel, Department of Applied Physics and Photonics, Brussels Photonics (B-PHOT) and Flanders Make, Pleinlaan 2, 1050 Brussels, Belgium
artemii.tishchenko@vub.be

Abstract: Optical fibers provide a favorable medium for nonlinear optical processes owing to the small mode field size and concurrently high optical intensity combined with the extended interaction lengths. Second harmonic generation (SHG) is one of those processes that has been demonstrated in silica glass optical fibers. Since silica is centrosymmetric, generating SHG in an optical fiber requires poling of the glass. In addition and when one wants to use ultrashort pulses for SHG, achieving both phase and group velocity matching is crucial. Although fibers that feature either modal phase velocity or group velocity matching for SHG have been reported, the possibility of simultaneous modal phase and group velocity matching was never reported before. In this paper we address this challenge, and for the first time to our knowledge, we show that it is feasible to do so with silica microstructured optical fibers featuring at least one ring of air holes in the cladding and a heavily Germanium doped core (above 25 mol.%) by exploiting the $LP_{01}(\omega)$ and $LP_{02}(2\omega)$ modes at 1.06 µm pump and 0.53 µm second harmonic wavelengths. This finding can greatly impact applications requiring waveguide based SHG generation with ultrashort pulses, including microscopy, material characterization and nonlinear imaging.

1. Introduction

Second Harmonic Generation (SHG) is a nonlinear optical process in which a pair of photons at identical frequencies interact with a nonlinear material and form a new photon at twice the pump frequency. Shortly after the invention of the laser, SHG emerged as an important technique for several applications. Besides providing an efficient means to generate coherent light at new and short wavelengths, SHG has been used for the characterization of the amplitude and phase of ultrashort pulses [1–3], as well as for the characterization of crystalline materials, more specifically for spotting conglomerates [4,5], for monitoring the formation of phase diagrams [6,7] and for studying the symmetry properties of crystals [8,9]. More recently, SHG has been applied to in-vivo biological imaging, where it allows identifying collagen structures in view of supporting early diagnosis of cancer [10–14]. This technique relies on the use of ultrashort-pulsed lasers, which calls for addressing specific challenges that stem from the broadband nature of the signal [1–3,8–12,14].

The first and the most important condition for enabling efficient SHG in a non-linear medium is to establish phase matching between the pump and the second harmonic wave. In addition, for ultrashort pulses, the group velocity mismatch limits the interaction length and thus the SHG conversion efficiency [15]. Achieving both phase matching and zero group velocity mismatch (zero-GVM) are therefore critical for SHG with ultrashort pulses [16]. This has been demonstrated

#453844 https://doi.org/10.1364/OE.453844
Journal © 2022 Received 26 Jan 2022; revised 18 Mar 2022; accepted 18 Mar 2022; published 25 Mar 2022

Optics EXPRESS

in several nonlinear crystals such as PPKN, PPLN, and β-BaB_2O_4 by means of quasi-phase matching (QPM) [17–20]. However, QPM requires tuning of the quadratic nonlinearity with a periodic poling technique which also limits the size of the crystal and thus the interaction length.

Alternatively, SHG in optical fibers has been long considered as it can allow for longer interaction lengths. Even though the silica glass from which optical fibers are manufactured features inversion symmetry and therefore a negligible second-order nonlinearity, SHG in optical fibers has been demonstrated for the first time in 1986 by means of self-induced poling of the doped core regions. Such a technique is referred to as all-optical poling [21]. In this process, a grating is formed by the interference of the pump with the second harmonic light, which in its turn forces positive and negative charges to move to opposite sides of the fiber core, leading to the existence of a static electric field along the fiber length and breaking of the inversion symmetry. SHG in optical fibers with electrical and thermal poling mechanisms has been demonstrated as well [22]. In optical fibers, QPM with periodic poling was used. However, and essentially similarly to SHG in bulk materials, periodic poling limits the fiber sample length and complicates the preparation of the nonlinear medium. In an alternative route, modal phase matching (MPM) was introduced to achieve phase-matching by using different modes of the fiber for the pump and harmonic signals [23]. MPM in standard step-index fibers can be achieved, for example, by tapering standard multi-mode fiber [24] and by using higher order modes [25–28]. Periodic poling of the quadratic nonlinearity is then not required. Moreover, the small efficiency of MPM due to limited mode overlap can be compensated by increasing the fiber length to some extent.

The introduction of microstructured optical fibers (MOF) marked an important milestone for enforcing SHG in optical fibers owing to the unprecedented design flexibility offered by the holey cladding of such fibers. More particularly, it was shown that hexagonal lattice microstructured fibers can achieve zero-GVM between the pump and the second harmonic signals across a wide range of cladding parameters. As a result, temporal walk-off can be avoided even for ultrashort pulse conversion, which infers broader spectral coverage of the SHG process [29]. Several MOFs enabling MPM for SHG were reported using either plain silica glass [30], high index inclusions embedded in silica glass [31] or chalcogenide glass [27]. Efficient SHG has also been demonstrated in hollow core Xe-filled MOF. For the latter, the Xe-gas pressure was changed to tune the modal properties of the fiber so as to satisfy the phase matching condition and to achieve efficient SHG [25]. Nonetheless, simultaneous MPM and zero-GVM for SHG in fibers has not yet been reported.

In this article we identify a wide range of microstructured fiber designs that allow simultaneously achieving MPM and zero-GVM for SHG. These fibers feature a standard hexagonal lattice of airholes in the cladding and a relatively high refractive index region in the core doped with Germanium. Our case study applies to pump and second harmonic wavelengths of 1.06 μm and 0.53 μm, respectively, but our approach can be extended to other wavelengths in the near infrared region. Note that although the required Ge-doping level is relatively high, MOFs with such a doping level were already successfully demonstrated for nonlinear applications [32–34].

Our paper is structured as follows: in Section 2 we introduce the fiber designs under study and their main properties. Section 3 deals with the unique dispersion properties of the heavily Ge-doped microstructured fibers with double MPM and double GVM points. Section 4 describes a design technique for simultaneous MPM and zero-GVM. In Section 5, we show the possibility of tuning the microstructure geometry at which MPM and zero-GVM are achieved by means of tailoring the doping level of the core region. In Section 6 we discuss and position our results with respect to the state-of-the-art. The last section contains concluding remarks.

2. Methods

We start our numerical study by considering two silica fiber configurations illustrated in Fig. 1: a step-index fiber and a MOF with a single ring of 6 air holes in a hexagonal configuration, both

Optics EXPRESS

with a Ge-doped region in the core. The main MOF cladding parameters are the air hole pitch (Λ), air hole diameter (d) and the resulting air filling factor ($AFF = d/\Lambda$). We also consider the doping level and the radius of the doped core region as design parameters. In particular, we focus on fibers with heavily Ge-doped cores (GeO_2 concentrations above 25 mol.%) similar to the ones that have already been successfully used for other nonlinear applications, such as four wave mixing and supercontinuum generation [33,34].

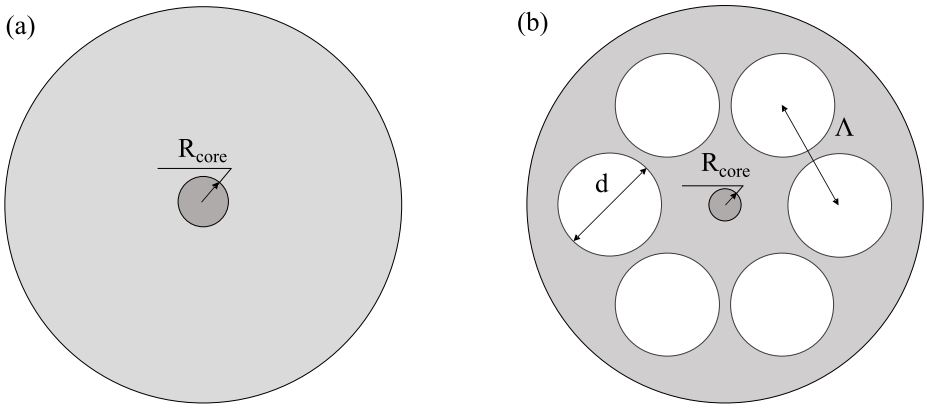

Fig. 1. Schematic illustrations of: (a) a step-index fiber and (b) a single-ring hexagonal lattice MOF with a heavily Ge-doped region.

We work with a pump wavelength of 1.06 μm, which is the Nd:YAG laser wavelength that is traditionally used for such purposes. Most of our results, however, can be adapted to other wavelengths in the near infrared region. For the modeling of the dispersion properties of the fibers we used a Device MODE Simulator from ANSYS/Lumerical Inc. [35]. For mode analysis we defined a simulation region that covers the extended core region of the fiber: doped core, air holed cladding and the surrounding silica glass. We implemented perfectly matched layer (PML) conditions at the boundaries. We preformed convergence tests on the size of the boundary region to make sure that the PML has minimal influence on the simulation results. The refractive indices of the Ge-doped and pure silica glasses materials were calculated from Sellmeier equations [36]. To validate our approach, we first modeled MOFs intended for zero-GVM as presented by Bache et al. [29] using a pure silica core hexagonal lattice MOFs, while assuming QPM. We verified the design for a 1.06 μm pump wavelength. The geometrical parameters for a zero-GVM MOF identified in [29] are as follows: $AFF = 0.72$; $\Lambda = 0.85$ μm and $d = 0.612$ μm. Our approach returns an identical AFF with air hole pitch and air hole diameter values $\Lambda = 0.846$ μm and $d = 0.609$ μm. These agree therefore very well with those in [29]. We also verified and compared the zero-GVM bandwidth of this MOF design. The value reported in [29] was $\Delta\lambda = 77$ nm for a corresponding Gaussian pulse width $\tau = 21$ fs. Our model (see calculation approach in Chapter 5) yields $\Delta\lambda = 61$ nm for $\tau = 27$ fs, which is in very reasonable agreement with [29].

A key characteristic of the SHG process is the conversion efficiency η, which can be expressed as follows [37]:

$$\eta = P\, l_F^2\, sinc^2\left(\frac{\Delta\beta l_F}{2}\right)\frac{1}{A_{ovl}}\,\frac{2\omega^2 d^2}{n_{eff}^{2\omega}(n_{eff}^{\omega})^2 c^3 \varepsilon_0} \times 100\%, \tag{1}$$

where P is the power of the pump beam; l_F is the fiber length, $\Delta\beta$ is the phase mismatch expressed by means of propagation constants (detailed below with Eq. (3)); A_{ovl} is the effective area that depends on the overlap integral between the interacting fields; ω is the angular frequency of the pump light; $d = \chi^{(2)}/2\pi$ is the nonlinearity factor, which includes the second order susceptibility

Optics EXPRESS

$\chi^{(2)}$; n_{eff}^{ω} and $n_{\text{eff}}^{2\omega}$ are the effective refractive indexes of the pump and second harmonic modes in the fiber respectively; c is the speed of light and ε_0 is the permittivity of vacuum.

The SHG conversion efficiency can thus be increased not only by increasing the pump power P, but also by reducing the effective area A_{ovl}, and increasing the fiber length l_{F}. First, we can decrease A_{ovl} by selecting adequate modes, since it is defined as [38]:

$$A_{ovl} = \left| \iint E^{*}_{SHG} E^{2}_{pump} dxdy \right|^{-2}, \tag{2}$$

where E_{pump} and E_{SHG} are the normalized mode profiles of the pump and the second harmonic modes, respectively. A non-zero effective area can hence be obtained by exploiting modes featuring an identical symmetry. In our study, we consider the fundamental $LP_{01}(\omega)$ mode for the pump and the higher order $LP_{02}(2\omega)$ mode for the second harmonic. Note that this mode pair has been frequently exploited in literature on nonlinear optics with optical fibers [25–27,39,40]. The effective area for the mode pair $LP_{01}(\omega)$ and $LP_{02}(2\omega)$ has the smallest non-zero value right after that of the pair formed by $LP_{01}(\omega)$ and $LP_{01}(2\omega)$. Second, we can increase the useful fiber length by tailoring the dispersion properties of the propagation constants of the fiber. To understand this, we express the phase matching condition (phase and group velocities) as a Taylor expansion of the phase mismatch of the propagation constants $\Delta\beta$ around the central pump frequency ω_0:

$$\begin{aligned} \Delta\beta(\omega_0) = {} & \beta(2\omega_0) - 2\beta(\omega_0) \\ & + 2(\omega-\omega_0)\left(\frac{\partial\beta(2\omega_0)}{\partial\omega} - \frac{\partial\beta(\omega_0)}{\partial\omega}\right) \\ & + (\omega-\omega_0)^2\left(\frac{\partial^2\beta(2\omega_0)}{\partial\omega^2} - \frac{1}{2}\frac{\partial^2\beta(\omega_0)}{\partial\omega^2}\right) + O(\omega-\omega_0)^n, \end{aligned} \tag{3a}$$

$$\begin{aligned} \Delta\beta(\omega_0) = {} & \frac{2}{c}\omega_0(n_{eff}^{2\omega} - n_{eff}^{\omega}) \\ & + \frac{2}{c}(\omega-\omega_0)(n_g^{2\omega} - n_g^{\omega}) \\ & + 2(\omega-\omega_0)^2\left(GVD_{\omega} - \frac{1}{2}GVD_{2\omega}\right) + O(\omega-\omega_0)^n, \end{aligned} \tag{3b}$$

In Eq. (3a) above, $\beta(\omega_0)$ and $\beta(2\omega_0)$ are the propagation constants of the pump and the second harmonic signals, respectively. ω_0 is the central angular frequency of the pump wave in the Taylor expansion. Equation (3a) can be rewritten as Eq. (3b), where $n_{\text{g}}^{2\omega}$ and n_{g}^{ω} correspond to the group indices of the second harmonic and pump wave. GVD_{ω}. and $GVD_{2\omega}$ are the group velocity dispersions. $O(\omega-\omega_0)^n$ refers to the higher order derivatives inside the Taylor expansion. Note that the first order derivative in the Taylor expansion corresponds to the inverse of the group velocity $v_{\text{g}} = \partial\omega/\partial\beta$, which we will express in terms of the group index: $n_{\text{g}} = c/v_{\text{g}}$.

The effective or useful fiber length or SHG is now limited by the coherence length (l_{coh}) and the temporal walk-off length (l_{w}). The coherence length depends on the first difference term in Eq. (3a) and is expressed as $l_{\text{coh}} = \pi/(\beta(2\omega_0) - 2\beta(\omega_0))$. It is thus inversely proportional to the mismatch between the propagation constants of the pump and the second harmonic and represents the fiber length over which the phase difference between the pump and second harmonic waves becomes π, which in its turn leads to back-conversion of the second harmonic into the pump frequency [41]. The difference $\beta(2\omega_0) - 2\beta(\omega_0)$ can be expressed by means of the corresponding effective refractive indices (see Eq. (3b)).

The second difference term in Eq. (3a), $\partial\beta(2\omega_0)/\partial\omega - \partial\beta(\omega_0)/\partial\omega$, relates to the group velocity mismatch (GVM), and defines the so-called temporal walk-off length. The latter can be written as $l_{\text{w}} = \Delta\tau/GVM$, where $\Delta\tau$ is the temporal pulse width and GVM is the group

Optics EXPRESS

velocity mismatch, which is in its turn defined as the difference of the inverse group velocities of the fundamental and second harmonic modes: $1/v_g^{\omega} - 1/v_g^{2\omega}$. The temporal walk-off length l_w quantifies the fiber length over which the pump and the second harmonic pulses spatially overlap. The group velocity mismatch or temporal walk-off can be expressed in terms of the corresponding group index difference (see Eq. (3b)).

When MPM and zero-GVM are achieved in a fiber, l_{coh} and l_w are no longer limiting the effective fiber length for SHG. The limit is then set by the higher order terms in Eq. (3a) and Eq. (3b). As we will show in Section 5, this allows considering ultrashort pulses since this significantly broadens the bandwidth of the SHG process [29,39].

3. Dispersion characteristics of heavily Ge-doped fibers

At this stage we can start with studying the dispersion characteristics of the fibers shown in Fig. 1 as a function of the design features. In the initial model, we consider a silica step-index fiber with a 36 mol.% Ge-doped core region and a pump signal at a 1.06 μm wavelength. Note that this particular doping level was already used for nonlinear optics in heavily doped MOFs [33,34,42].

We initiated our study by considering the dependence of the phase and group velocity in a regular step-index fiber (expressed by ways of n_{eff} and n_g) on the radius of the doped core region, which is shown in Fig. 2(a) and 2(b). Figure 2(a) shows that it is possible to match the effective refractive indices of the $LP_{01}(\omega)$ and $LP_{02}(2\omega)$ modes of the pump and the second harmonic respectively, and hence to achieve MPM, by changing the radius of the doped core region. However, group velocity matching between the $LP_{01}(\omega)$ and $LP_{02}(2\omega)$ modes is not achieved. Figure 2(b) shows that for a small core radius, i.e. for a low value of R_{core}, the fiber enters single-mode operation, which prevents the intersection of the $LP_{01}(\omega)$ and $LP_{02}(2\omega)$ curves. The cut-off radius for this step-index fiber is shown with a dashed vertical line in Fig. 2(a) and 2(b).

Let us now consider the MOF shown in Fig. 1(b), which is obtained by adding a single ring of air holes with AFF = 0.9 and $\Lambda = 2.75$ μm to the step-index fiber design. The results for n_{eff} and n_g are shown in Fig. 2(c) and 2(d) respectively. The MOF behaves in a similar manner as the step-index fiber above the cut-off radius of the latter. However, the properties of the higher order LP_{02} mode are notably different. Owing to the microstructure, the LP_{02} mode still exists for smaller doped core regions and a second MPM point appears as shown in Fig. 2(c). Remarkably, the group refractive index curves for the pump and the second harmonic wavelengths demonstrate a comparable behavior for smaller doped core sizes and we observe 2 zero-GVM points as shown on Fig. 2(d). To the best of our knowledge, this is the first report about the existence of 2 MPM and 2 zero-GVM points for $LP_{01}(\omega)$ and $LP_{02}(2\omega)$ modes in any type of optical fiber or waveguide intended for SHG.

To understand the appearance of the 2nd MPM and the 2nd zero-GVM points, we consider the mode intensity distribution patterns for the MOF $LP_{01}(\omega)$ and $LP_{02}(2\omega)$ modes as shown in Fig. 3. The MOF design modeled here has a doped core radius of 0.450 μm, an air hole pitch of 2.75 μm and an AFF of 0.9. Such a small core region is well within the reach of modern fabrication technologies. In [34], for example, the authors demonstrated a MOF with a 36 mol.% Ge-doping level and with a doped core radius of 0.325 μm. Owing to the presence of the air holes in the cladding region, we have multimode guidance and a well confined $LP_{02}(2\omega)$ mode (see Fig. 3(b)). Whilst the $LP_{01}(\omega)$ mode is mostly located in the doped region (see Fig. 3(a)), the $LP_{02}(2\omega)$ mode has a central intensity distribution across the doped region and a higher order mode ring-shaped intensity distribution in the pure silica portion, between the doped region and the holey cladding. As R_{core} decreases, the $LP_{02}(2\omega)$ mode has a larger overlap with the pure silica region with lower refractive index than the doped region. This eventually allows observing the 2nd MPM and 2nd zero-GVM points.

Optics EXPRESS

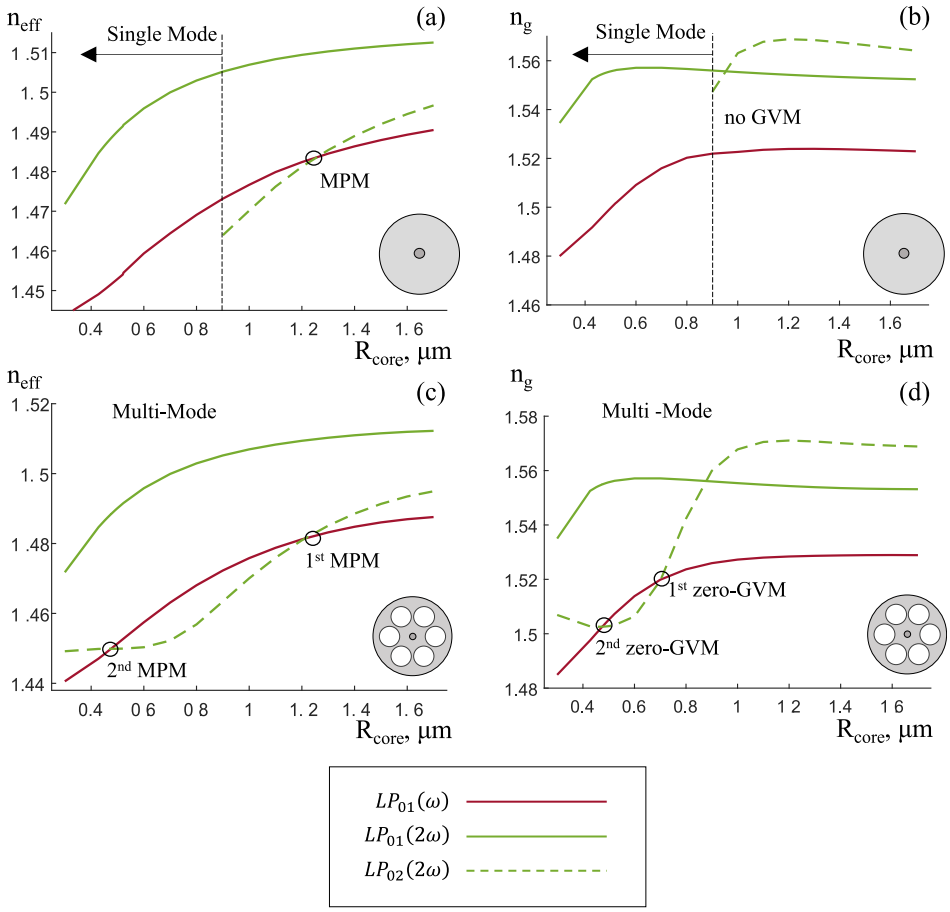

Fig. 2. The dependence of the effective refractive index ((a) and (c)) and the group index ((b) and (d)) of the LP_{01} mode at 1.06 μm and of the LP_{02} mode at 0.53 μm in a step-index fiber ((a) and (b)) and in a MOF ((c) and (d)) on the radius of the 36 mol.% Ge-doped core region. The MOF has an air hole pitch $\Lambda = 2.75\ \mu m$ and an AFF = 0.9.

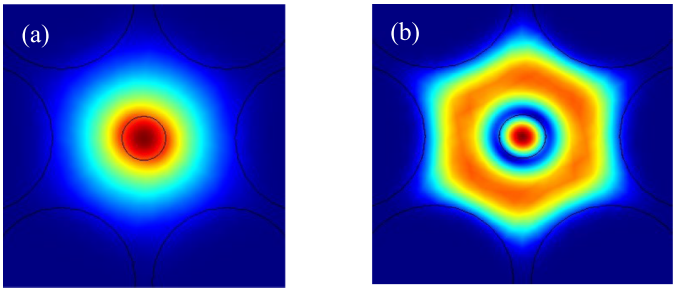

Fig. 3. Normalized electric field distribution of: (a) fundamental LP_{01} and (b) second harmonic LP_{02} modes for a MOF with an air hole pitch $\Lambda = 2.75\ \mu m$ and an AFF = 0.9

Optics EXPRESS

4. Simultaneous MPM and zero-GVM in a MOF

We now take further advantage of the conclusion that the 2nd MPM and 2nd zero-GVM points demonstrated in the previous section appear for R_{core} values of the doped core that are close to each other. To investigate the possibility of achieving the 2nd MPM and 2nd zero-GVM points for the same fiber design, we check what happens when we adapt the air hole pitch Λ of the microstructured cladding for a fixed AFF = 0.9. For each value of Λ, we can identify for which R_{core} we find MPM and zero-GVM. This is illustrated in Fig. 4, which considers airhole pitches larger than the initial $\Lambda = 2.75$ µm. As we increase the airhole pitch, the 2nd MPM point shifts towards larger doped core radii. At the same time, the 2nd zero-GVM point shifts towards smaller doped core radii. This allows identifying a combination of airhole pitch and doped core radius values for which we have simultaneous MPM and zero-GVM. Figure 4 reveals such a MOF design (marked with a star) obtained with Λ=3.075 µm and $R_{core} = 0.473$ µm. To the best of our knowledge, this is the first report of a MOF design intended for SHG that features simultaneous MPM and zero-GVM.

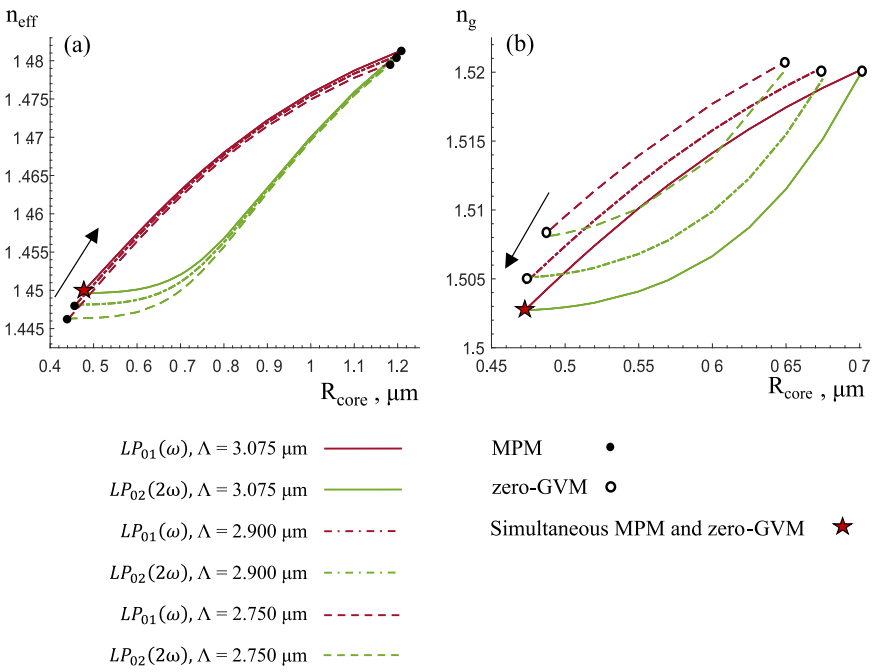

Fig. 4. (a) Effective refractive index as a function of the doped core region radius and (b) group index as a function of the doped core region radius for different values of the air hole pitch and fixed AFF = 0.9. The plots allow visualizing for which designs MPM (a) and zero-GVM (b) are obtained, and for which particular design simultaneous MPM and zero-GVM is found. The arrows indicate the direction of the shift of the MPM points (a) and zero-GVM points (b) with increasing air hole pitch. Note: arrows on graphs show shift in MPM or zero-GVM while Λ increases

5. Simultaneous MPM & zero-GVM for different Ge-doping levels and MOF air filling factors

Starting from our strategy for identifying MOF designs with simultaneous MPM and zero-GVM outlined above, we can now investigate whether we can obtain such MOF designs for other Ge-doping concentrations as well. In other words, we take different fixed doping levels, we keep

Optics EXPRESS

the AFF = 0.9 constant and we identify Λ and R_{core} combinations that allow for simultaneous MPM and zero-GVM with the approach explained in Section 4. The dependencies of n_{eff} and n_g on the doped core radius are shown in Fig. 5 for core doping levels of 25, 36 and 50 mol.%. The designs for which we find simultaneous MPM and zero-GVM are indicated with a star. We can see that decreasing the doping level brings the 2nd MPM and 2nd zero-GVM points closer to each other. For the 50 mol.% Ge-doped core, the difference between the core radii of the double MPM points is 0.79 µm, while for 25 mol.% it is 0.54 µm (see Fig. 5(a)). For the double zero-GVM points the difference in core radii for 50 mol.% is 0.27 µm, while for 25 mol.% it is 0.09 µm (see Fig. 5(b)). Since this last value is very small, 25 mol.% level can be considered as a lower limit for achieving simultaneous MPM and zero-GVM. For MOFs with lower Ge-doping levels, we can achieve simultaneous MPM and zero-GVM points with larger core radii, which can be important in view of easing the manufacturability of the fiber.

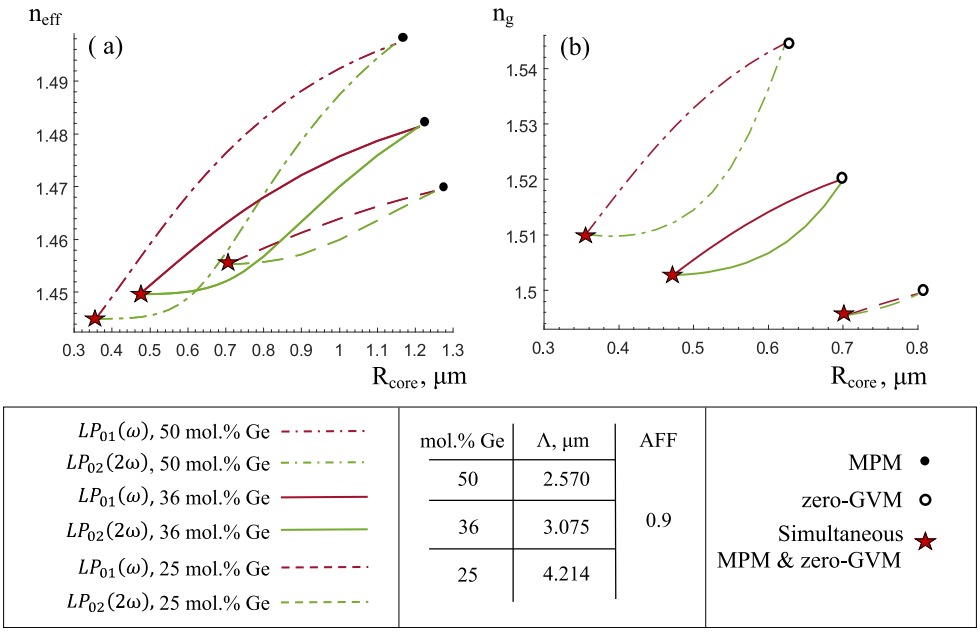

Fig. 5. (a) Effective refractive index as a function of the doped core region radius and (b) group index as a function of the doped core region radius for different values of the Ge-doping level and a fixed AFF = 0.9. The plots allow visualizing for which designs simultaneous MPM and zero-GVM are obtained.

We can also consider the influence of the AFF. Our simulations show that for a fixed Ge-doping level, decreasing the AFF from 0.9 to 0.8 and 0.7 calls for smaller pitch values to achieve simultaneous MPM and zero-GVM. This is shown in Fig. 6(a) for different Ge-doping levels of the core. Note that for each configuration, the air hole size is different, but there is little influence on the optimal R_{core} size (±1 nm). AFF values below 0.7 did not allow for modal phase matching for smaller size cores. Figure 6 clearly reveals that the largest size of the air hole pitch Λ = 4.214 µm for simultaneous MPM and zero-GVM is obtained with a 25 mol.% doping level and AFF = 0.9.

Figure 6(b) shows the different MOF designs superimposed onto each other for a fixed doping level of the doped core region radius. It is remarkable that these geometries for simultaneous MPM and zero-GVM are such that the radius $\Lambda(1 - AFF/2)$ of the circle delimiting the location of the inner boundaries of the air holes drawn in blue in Fig. 6(b) remains quasi constant. By

Optics EXPRESS

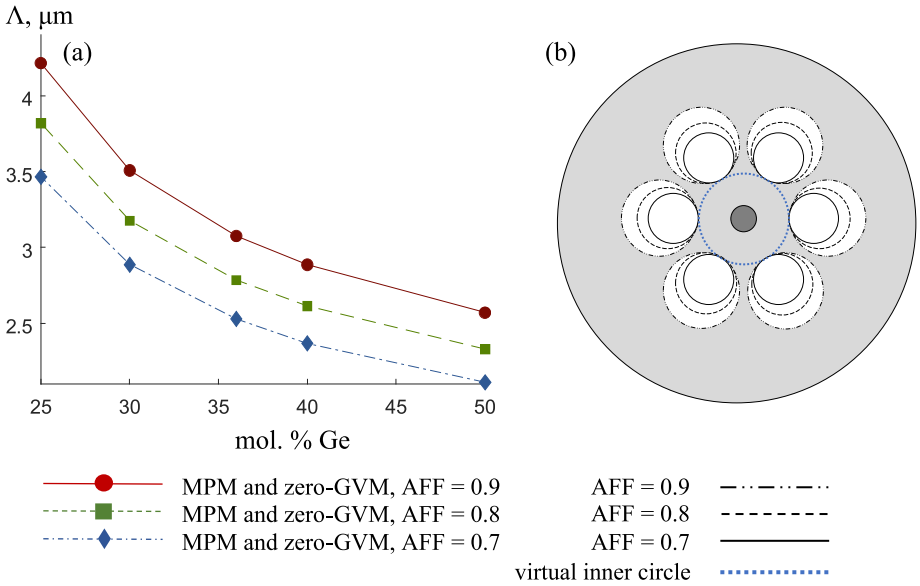

Fig. 6. (a) Simultaneous MPM and zero-GVM points for different Λ — AFF and doping level combinations and (b) illustration of the superimposed MOF geometries concept for a fixed doping level.

using the radius of this circle, it is possible to find MPM and zero-GVM MOF designs for different AFFs, once one design is computed.

Note that we have also studied hexagonal lattice MOFs with more airhole rings and found that the additional rings have negligible influence on the simultaneous MPM and zero-GVM fiber design parameters.

Table 1 summarizes our results for MOFs featuring simultaneous MPM & zero-GVM and compiles the design parameters of the fibers with the results of the calculations of the effective area and the corresponding SHG bandwidth for a central pump wavelength of 1.06 μm. The latter is defined as the wavelength range over which the $sinc^2(\Delta\beta/L)$ factor in the expression for the SHG conversion efficiency (Eq. (1)) remains $\geq$ 0.5, when considering fiber lengths of 10 cm [29,38]. This value should be considered as an upper limit for the bandwidth of the ultrashort pulses for which these conditions would be fulfilled. The calculated SHG bandwidths are in the range of tens of nanometers, which correspond to pulse lengths down to the femtosecond range (for a Gaussian pulse shape). For example, a MOF with 36 mol.% Ge and AFF = 0.9 has a bandwidth of 23.4 nm, which corresponds to a Gaussian pump pulse with a duration of about 70 fs. For sake of comparison, we note that in standard step index fibers the bandwidth for $LP_{01}(\omega)$ – $LP_{02}(2\omega)$ SHG conversion for a pump wavelength of 1.06 μm is only 0.1 nm due to the high value of the GVM around 82 fs/mm. For a Gaussian pulse this corresponds with a pulse width of 16 ps, which is more than two orders of magnitude larger than the values presented for our MOF designs.

Optics EXPRESS

Table 1. List of MOF designs featuring simultaneous MPM and zero-GVM

AFF	mol. % Ge	Λ, µm	$R_{air\ hole}$, µm	R_{core}, µm	A_{ovl}, μm^2	[a]BW, nm
0.9	50	2.570	1.157	0.356	9.06	11.5
	40	2.885	1.298	0.429	11.55	31.1
	36	3.075	1.384	0.473	13.19	23.4
	30	3.507	1.578	0.568	17.26	12.3
	25	4.214	1.896	0.706	24.05	12.1
0.8	50	2.329	0.931	0.356	9.10	11.5
	40	2.613	1.045	0.429	11.58	31.7
	36	2.784	1.114	0.472	13.21	23.1
	30	3.176	1.270	0.567	17.27	12.3
	25	3.818	1.527	0.705	24.04	12.1
0.7	50	2.112	0.739	0.355	9.24	11.6
	40	2.367	0.828	0.428	11.63	38.4
	36	2.529	0.885	0.471	13.34	23.8
	30	2.888	1.011	0.567	17.46	12.1
	25	3.465	1.213	0.704	24.14	12.1

[a]The bandwidth is calculated for a fiber length $l_F = 10$ cm

6. Discussion

Since the first demonstration of SHG by Franken et al. [43], the research efforts in this domain aimed essentially to increase the conversion efficiency. As a result, several classical phase matching concepts were developed: MPM [28], all-optical poling (AOP) [44] and QPM [22,45]. With the introduction of ultrashort pulse lasers, the community focused on group-velocity matching as another important dispersion mechanism that allows for conversion with a broader bandwidth. Research efforts therefore turned to investigating structures in which both phase- and group velocity matching can support effective ultrashort pulse conversion. One pioneering idea was proposed by Zhang et al. [17], where noncollinear pulses were phase- and group velocity matched in a nonlinear crystal. However, limitations imposed by the relatively short crystal length and by the complicated optical setups called for developing more efficient concepts. In the meantime, for fiber- and waveguide-based applications, QPM with a zero-GVM [19,20,29] and AOP with a zero-GVM [46] had appeared as alternatives. Nonetheless, in the case of QPM, external poling by means of periodically arranged electrodes still limits the fiber length and complicates the preparation of the nonlinear medium. Like crystals, waveguides exploiting QPM or AOP have a relatively small interaction length resulting in a limited overall SHG efficiency. AOP can be considered as an extension of QPM, where periodic poling is implemented by means of light. The effective nonlinear coefficient is modulated over a period which is twice of the coherence length. This fundamental limitation can be overcome only in the case of equal phase-velocities or, in other words, in the case of MPM.

With our work, we show for the first time that MPM and zero-GVM are feasible in optical waveguides – and in our approach in optical fibers – for SHG. While we demonstrate this matching in a MOF here, it can be generalized to optical waveguides assuming the existence of double MPM with double zero-GVM points between the $LP_{01}(\omega)$ pump and $LP_{02}(2\omega)$ second harmonic modes.

Note first though that our finding of double phase matching points for SHG shows similarities with previously reported results in the field of nonlinear optics. For example, double phase matching for third order nonlinear processes was predicted by Tsvetkov et al. in a narrow range

Optics EXPRESS

of Ge-doping levels (23.44–23.77 mol.%) in a step-index fiber, and this between the $HE_{11}(\omega)$ pump and $HE_{13}(3\omega)$ third harmonic modes [23]. It is remarkable that such a narrow range of Ge-doping concentrations required for the double phase matching in [23] was mostly limited by the higher order mode's cutoff point. Our study extends well on the possibility of obtaining double MPM points, this time for SHG rather than for a third order nonlinear process, and as stated before, the appearance of double matching points in view of efficient ultrashort-pulse laser-based SHG is reported for the first time to the best of our knowledge. We show that double phase matching points in a small core fiber appear when relatively high Δn condition is applied for: a) Ge-doped core — surrounding silica region and b) doped core surrounding silica region — air holed cladding.

Second, note also that the possibility for achieving zero-GVM between different fiber modes with an identical symmetry and at the same time MPM was experimentally shown by Demas et al. for the third-order nonlinear process of four-wave mixing [39]. MPM between the high-order LP_{04} and LP_{05} modes (for pump — anti-Stokes and pump — Stokes pairs respectively), resulted in a zero-GVM between the anti-Stokes — Stokes pair. Our study, however, shows simultaneous MPM and zero-GVM in the cases where the pump is the fundamental LP_{01} mode and the second-order nonlinear process generates light in the LP_{02} mode. Our use of low-order modes simplifies the intermodal group-velocity matching scheme, here applied to SHG for the first time as well.

Finally, whilst available literature has reported many times on either phase velocity — or group velocity matching, our work manifests the possibility of simultaneous MPM and zero-GVM for SHG in a single fiber design. The leitmotif for achieving MPM is to enable the nonlinear process over much longer interaction lengths. MPM, in contrast to QPM, does not need any periodically induced nonlinearity, which simplifies fiber preparation. A standard thermal poling over the whole fiber length can still be used for breaking glass symmetry. In addition to MPM, zero-GVM increases the SHG bandwidth, which allows for ultrashort pulse conversion. Such ultrashort second harmonic pulse generation is much sought after in view of pushing the frontiers of material science and in-vivo bio-imaging applications. Simultaneous MPM with zero-GVM as reported in our paper fills a gap in the search for methods on simultaneous phase- and group-velocity matching for SHG as shown previously for QPM with zero-GVM and AOP with zero-GVM.

7. Conclusion

We have studied phase matching and group velocity matching for SHG in heavily Ge-doped microstructured optical fibers. First, we have identified, for the first time to our knowledge, the existence of two MPM and two zero-GVM points between the $LP_{01}(\omega)$ pump and $LP_{02}(2\omega)$ second harmonic modes. Second, we have shown that by tuning the microstructure parameters, simultaneous MPM and zero-GVM are possible. Such microstructured fibers could impact fiber-based SHG by providing unique phase-matching conditions over extended interaction lengths. In practice, this would enable SHG with ultrashort pulse lengths down to the femtosecond range. Finally, and most importantly, our parameter study evidences that such properties are achievable with a wide range of MOF designs with features that are well within established fabrication limits.

Funding. Flanders (FWO) (12P1720N, EOS ID 30467715); FWO Hercules Foundation–Flanders; Methusalem Foundation; OZR of Vrije Universiteit Brussel; Industrial Research Fund; Interreg (NWE758, Fotonica pilootlijnen).

Acknowledgments. The authors wish to acknowledge financial support by Research Foundation—Flanders (FWO) by ways of EOS Project G0F6218N (EOS ID 30467715). Interreg (NWE758, Fotonica pilootlijnen), Industrial Research Fund (IOF), OZR of Vrije Universiteit Brussel, Methusalem Foundation, the FWO Hercules Foundation–Flanders are acknowledged as well. Tigran Baghdasaryan is a postdoctoral Fellow of the Research Foundation—Flanders (FWO 12P1720N).

Disclosures. The authors declare no conflicts of interest.

Optics EXPRESS

Data availability. Data underlying the results presented in this paper are not publicly available at this time but may be obtained from the authors upon reasonable request.

References

1. A. Watanabe, S. Tanaka, H. Kobayashi, Y. Ishida, and T. Yajima, "Microcomputer-based spectrum-resolved second-harmonic generation correlator for fast measurement of ultrashort pulses," Rev. Sci. Instrum. **56**(12), 2259–2262 (1985).
2. C. Janisch, N. Mehta, D. Ma, A. L. Elías, N. Perea-López, M. Terrones, and Z. Liu, "Ultrashort optical pulse characterization using WS_2 monolayers," Opt. Lett. **39**(2), 383–385 (2014).
3. E. Dai, C. Zhou, and G. Li, "Dammann SHG-FROG for characterization of the ultrashort optical pulses," Opt. Express **13**(16), 6145–6152 (2005).
4. A. Galland, V. Dupray, B. Berton, S. Morin-Grognet, M. Sanselme, H. Atmani, and G. Coquerel, "Spotting conglomerates by second harmonic generation," Cryst. Growth Des. **9**(6), 2713–2718 (2009).
5. F. Simon, S. Clevers, V. Dupray, and G. Coquerel, "Relevance of the Second Harmonic Generation to Characterize Crystalline Samples," Chem. Eng. Technol. **38**(6), 971–983 (2015).
6. S. Clevers, F. Simon, M. Sanselme, V. Dupray, and G. Coquerel, "Monotropic transition mechanism of m-hydroxybenzoic acid investigated by temperature-resolved second harmonic generation," Cryst. Growth Des. **13**(8), 3697–3704 (2013).
7. L. Yuan, S. Clevers, A. Burel, P. Negrier, M. del Barrio, B. ben Hassine, D. Mondieig, V. Dupray, J. L. Tamarit, and G. Coquerel, "New Intermediate Polymorph of 1-Fluoro-adamantane and Its Second-Order-like Transition toward the Low Temperature Phase," Cryst. Growth Des. **17**(6), 3395–3401 (2017).
8. J. Ribeiro-Soares, C. Janisch, Z. Liu, A. L. Elías, M. S. Dresselhaus, M. Terrones, L. G. Cançado, and A. Jorio, "Second harmonic generation in WSe_2," 2D Mater. **2**(4), 045015 (2015).
9. L. Mennel, M. Paur, and T. Mueller, "Second harmonic generation in strained transition metal dichalcogenide monolayers: MoS_2, $MoSe_2$, WS_2, and WSe_2," APL Photonics **4**(3), 034404 (2019).
10. X. Chen, O. Nadiarynkh, S. Plotnikov, and P. J. Campagnola, "Second harmonic generation microscopy for quantitative analysis of collagen fibrillar structure," Nat. Protoc. **7**(4), 654–669 (2012).
11. V. Ajeti, O. Nadiarnykh, S. M. Ponik, P. J. Keely, K. W. Eliceiri, and P. J. Campagnola, "Structural changes in mixed Col I/Col V collagen gels probed by SHG microscopy: implications for probing stromal alterations in human breast cancer," Biomed. Opt. Express **2**(8), 2307–2316 (2011).
12. A. Keikhosravi, J. S. Bredfeldt, A. K. Sagar, and K. W. Eliceiri, "Second-harmonic generation imaging of cancer," Methods in Cell Biol. **123**, 531–546 (2014).
13. K. Burke and E. Brown, "The Use of Second Harmonic Generation to Image the Extracellular Matrix During Tumor Progression," Intravital **3**(3), e984509 (2014).
14. R. A. Natal, J. Vassallo, G. R. Paiva, V. B. Pelegati, G. O. Barbosa, G. R. Mendonça, C. Bondarik, S. F. Derchain, H. F. Carvalho, C. S. Lima, C. L. Cesar, and L. O. Sarian, "Collagen analysis by second-harmonic generation microscopy predicts outcome of luminal breast cancer," Tumor Biol. **40**(4), 101042831877095 (2018).
15. W. Han, W. G. Zheng, Y. S. Yang, D. X. Cao, Q. H. Zhu, and L. J. Qian, "Phase matching limitation of high-efficiency second-harmonic generation in both phase- and group-velocity-matched structures," Optik **119**(3), 122–126 (2008).
16. X. Xiao, C. Yang, S. Gao, and H. Miao, "Analysis of ultrashort-pulse second-harmonic generation in both phase- and group-velocity-matched structures," IEEE J. Quantum Electron. **41**(1), 85–93 (2005).
17. T. R. Zhang, R. Choo, and M. C. Downer, "Phase and Group Velocity Matching for Second Harmonic Generation of Femtosecond Pulses," Appl. Opt. **29**(27), 3927–3933 (1990).
18. J. Huang, J. R. Kurz, C. Langrock, A. M. Schober, and M. M. Fejer, "Quasi-Group-Velocity Matching Using Integrated-Optic Structures," Opt. Lett. **29**(21), 2482–2484 (2004).
19. S. H. Bae, I. H. Baek, S. Y. Choi, W. B. Cho, F. Rotermund, and C. S. Yoon, "Efficient second-harmonic generation of ultrashort pulses with simultaneous quasi-phase matching and group velocity matching in periodic 90° domain structures of potassium niobate," Opt. Commun. **283**(9), 1894–1898 (2010).
20. J. Jiang, J. Zhang, K. Wang, X. Xiao, and Z. Zhang, "Broadband second-harmonic generation in APPLN with group-velocity matching," Opt. Commun. **403**, 217–221 (2017).
21. U. Osterberg and W. Margulis, "Dye Laser Pumped by Nd:YAG Laser Pulses Frequency Doubled in a Glass Optical Fiber," Opt. Lett. **11**(8), 516–518 (1986).
22. P. G. Kazansky and V. Pruneri, "Electric-Field Poling of Quasi-Phase-Matched Optical Fibers," J. Opt. Soc. Am. B **14**(11), 3170–3179 (1997).
23. S. Tsvetkov, K. Katamadze, N. Borshchevskaia, A. Sysolyatin, M. Fedorov, S. Kulik, M. Salganskii, and A. Belanov, "Phase-matching of the HE_{11} and HE_{13} modes of highly doped GeO_2-SiO_2 fiber waveguides at 1596 nm and 532 nm, respectively, for triple-photon generation," Laser Phys. Lett. **13**(2), 025104 (2016).
24. S. Richard, "Second-Harmonic Generation in Tapered Optical Fibers," J. Opt. Soc. Am. B **27**(8), 1504–1512 (2010).
25. J.-M. Ménard and P. St. J. Russell, "Phase-matched electric-field-induced second-harmonic generation in Xe-filled hollow-core photonic crystal fiber," Opt. Lett. **40**(15), 3679–3682 (2015).
26. J. F. Liao, J. Q. Sun, M. di Du, and Y. Qin, "Design of microstructured fibers for second-harmonic generation based on modal phase-matched technique," Optik **124**(24), 6950–6953 (2013).

Optics EXPRESS

27. F. Cao, P. Zhang, S. Dai, X. Wang, T. Xu, and Q. Nie, "Mid-infrared second-harmonic generation in chalcogenide photonic crystal fiber," Opt. Commun. **335**, 257–261 (2015).
28. M. E. Fermann, L. Li, M. C. Farries, and D. N. Payne, "Frequency-Doubling by Modal Phase Matching in Poled Optical Fibres," Electron. Lett. **24**(14), 894–895 (1988).
29. M. Bache, H. Nielsen, J. Laegsgaard, and O. Bang, "Tuning quadratic nonlinear photonic crystal fibers for zero group-velocity mismatch," Opt. Lett. **31**(11), 1612–1614 (2006).
30. J. Liao, J. Sun, M. Du, and Y. Qin, "Proposal for sum-frequency generation based on modal phase-matching in photonic crystal fibers," Opt. Fiber Technol. **20**(2), 90–94 (2014).
31. A. Bétourné, Y. Quiquempois, G. Bouwmans, and M. Douay, "Design of a Photonic Crystal Fiber for Phase-Matched Frequency Doubling or Tripling," Opt. Express **16**(18), 14255–14262 (2008).
32. T. Stefaniuk, G. Stępniewski, D. Pysz, R. Stępień, and R. Buczyński, "Fused silica photonic crystal fiber with heavily germanium doped microinclusion in the core dedicated to couple, guide and control LP02 higher-order mode," Opt. Express **26**(17), 21939–21949 (2018).
33. J. Kobelke, K. Schuster, D. Litzkendorf, A. Schwuchow, J. Kirchhof, V. Tombelaine, H. Bartelt, P. Leproux, V. Couderc, A. Labruyere, and R. Jamier, "Highly germanium and lanthanum modified silica based glasses in microstructured optical fibers for non-linear applications," Opt. Mater. **32**(9), 1002–1006 (2010).
34. A. Labruyére, P. Leproux, V. Couderc, V. Tombelaine, J. Kobelke, K. Schuster, H. Bartelt, S. Hilaire, G. Huss, and G. Mélin, "Structured-core GeO_2-doped photonic-crystal fibers for parametric and supercontinuum generation," IEEE Photonics Technol. Lett. **22**(16), 1259–1261 (2010).
35. "Lumerical," www.lumerical.com.
36. J. W. Fleming, "Dispersion in GeO_2-SiO_2 Glasses," Appl. Opt. **23**(24), 4486–4493 (1984).
37. V. Pruneri, G. Bonfrate, P. G. Kazansky, D. J. Richardson, N. G. Broderick, J. P. de Sandro, C. Simonneau, P. Vidakovic, and J. A. Levenson, "Greater than 20%-Efficient Frequency Doubling of 1532-nm Nanosecond Pulses in Quasi-Phase-Matched Germanosilicate Optical Fibers," Opt. Lett. **24**(4), 208–210 (1999).
38. T. M. Monro, V. Pruneri, N. G. R. Broderick, D. Faccio, P. G. Kazansky, and D. J. Richardson, "Broad-band second-harmonic generation in holey optical fibers," IEEE Photonics Technol. Lett. **13**(9), 981–983 (2001).
39. J. Demas, L. Rishøj, X. Liu, and G. Prabhakar, "Intermodal group velocity engineering for broadband nonlinear optics," Photonics Res. **7**(1), 1–7 (2019).
40. L. Xiao, C. Lin, W. Zhang, Y. Huang, and J. Peng, "Modal phase-matching second harmonic generation in Bragg fiber," Opt. Commun. **281**(9), 2614–2617 (2008).
41. A. J. Goodman and W. A. Tisdale, "Enhancement of second-order nonlinear-optical signals by optical stimulation," Phys. Rev. Lett. **114**(18), 183902 (2015).
42. K. Schuster, J. Kobelke, Y. Wang, A. Schwuchow, J. Kirchhof, H. Bartelt, and S. Pissadakis, "Highly photosensitive PCFs with extremely germanium doped core," in *AIP Conference Proceedings* **1288**, 47–51 (2010).
43. P. A. Franken, A. E. Hill, C. W. Peters, and G. Weinreich, "Generation of Optical Harmonics," Phys. Rev. Lett. **7**(4), 118–119 (1961).
44. R. H. Stolen and H. W. K. Tom, "Self-Organized Phase-Matched Harmonic Generation in Optical Fibers," Opt. Lett. **12**(8), 585–587 (1987).
45. P. Sarrafi, E. Y. Zhu, K. Dolgaleva, B. M. Holmes, D. C. Hutchings, J. S. Aitchison, and L. Qian, "Continuous-wave quasi-phase-matched waveguide correlated photon pair source on a III-V chip," Appl. Phys. Lett. **103**(25), 251115 (2013).
46. D. D. Hickstein, D. R. Carlson, H. Mundoor, J. B. Khurgin, K. Srinivasan, D. Westly, A. Kowligy, I. I. Smalyukh, S. A. Diddams, and S. B. Papp, "Self-organized nonlinear gratings for ultrafast nanophotonics," Nat. Photonics **13**(7), 494–499 (2019).